NeuroImage **14,** 1361–1369 (2001)
doi:10.1006/nimg.2001.0937, available online at http://www.idealibrary.com on IDEAL®

Voxel-Based Morphometry Using the RAVENS Maps: Methods and Validation Using Simulated Longitudinal Atrophy

Christos Davatzikos,* Ahmet Genc,* Dongrong Xu,* and Susan M. Resnick†

*Center for Biomedical Image Computing, Department of Radiology, Johns Hopkins University School of Medicine, Baltimore, Maryland 21287; †Laboratory of Personality and Cognition, National Institute on Aging, National Institutes of Health, Baltimore, Maryland 21224-6825

Received February 16, 2001; published online October 24, 2001

Statistical analysis of anatomical maps in a stereotaxic space has been shown to be a useful tool in population-based studies for quantifying local anatomical differences or changes, without *a priori* assumptions about the location and extent of the regions of interest. This paper presents an extension and validation of a previously published methodology, referred to as RAVENS, for characterizing regional atrophy in the brain. A new method for elastic, volume-preserving spatial normalization, which allows for accurate quantification of very localized atrophy, is used. The RAVENS methodology was tested on images with simulated atrophy within two gyri: precentral and superior temporal. It was found to accurately determine the regions of atrophy, despite their localized nature and the interindividual variability of cortical structures. Moreover, it was found to perform substantially better than the voxel-based morphology method of SPM'99. Improved sensitivity was achieved at the expense of human effort involved in defining a number of sulcal curves that serve as constraints on the 3D elastic warping.

INTRODUCTION

Magnetic resonance imaging (MRI) has been used in numerous *in vivo* anatomical studies of the brain. The vast majority of the studies have been based on the *a priori* definition of a number of regions of interest (ROIs), followed by measurements of tissue volumes within each ROI. (Throughout this paper we use the term ROI for either a two- or a three-dimensional region, the latter often called a volume of interest, or VOI.) This approach is extremely laborious, since it requires the manual definition of many ROIs on a large number of subjects, and it becomes almost impossible for sample sizes typically found in many modern studies. Moreover, ROI approaches are subject to interrater variability. These limitations might be overcome as automated methods for ROI generation emerge (Collins *et al.*, 1999). However, the most important limitation of ROI-based analyses is that the ROI must be defined in advance, so that a volumetric measurement can be taken. In practice, it is not known in advance which regions might be affected by disease. The affected region might be only part of a well-characterized anatomical region, such as a gyrus, or it might span different regions. To overcome these limitations of ROI analyses, alternative approaches which are based on point (voxel)-wise analysis have been developed in the past several years. In these methods, three-dimensional scalar or vector fields are first generated by spatially normalizing images from different subjects to a standardized template, such as a deterministic or probabilistic atlas, or even a single subject. A voxel-wise statistical analysis of the resulting scalar or vector fields subsequently determines regions in which there are significant group or condition differences. A commonly used example of these approaches is *statistical parametric mapping* (SPM) (Friston *et al.*, 1995a), which seeks regions of activation in functional images. Analogous methods have been used recently for studying anatomical images, and they fall under two categories: (1) methods that examine displacement vector fields that register a template of anatomy to a subject's own morphology and (2) methods that measure density of brain tissue or gray and white matter separately in a stereotaxic space, after spatial normalization.

Methods based on displacement fields have their roots in the seminal work by D'Arcy Thompson (1917), who visualized morphological differences between species by warping Cartesian grids from one species to the other. More modern work in that direction includes pattern theoretic approaches (Miller *et al.*, 1993, 1997; Christensen *et al.*, 1997), the point-wise analysis of deformation fields (determinant of the Jacobian) (Davatzikos *et al.*, 1996; Freeborough and Fox, 1998; Davatzikos and Resnick, 1998; Gaser *et al.*, 1999; Guimond *et al.*, 2000; Davatzikos, 2001), the use of principal components analysis (Briquer and Gee, 1997) or factor analysis (Machado *et al.*, 2000), and the use of local tensors representing anatomical variability voxel-wise (Thompson *et al.*, 1997, 2000). These approaches

1053-8119/01 $35.00

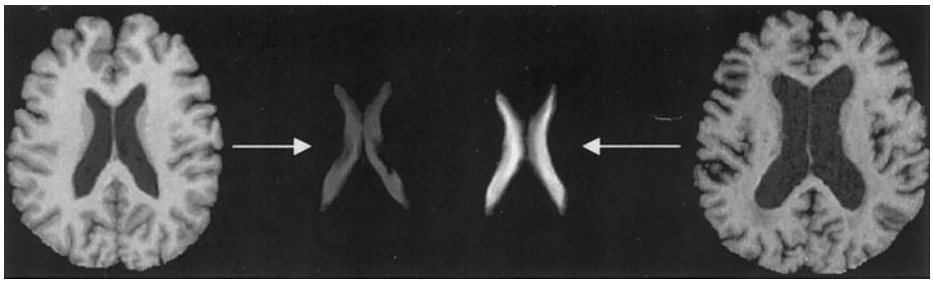

FIG. 1. MR images from two different subjects with different degrees of ventricular atrophy and their respective CSF RAVENS maps. Although the ventricles of the RAVENS maps have the same shape after elastic normalization, their brightness differs, reflecting the fact that relatively more CSF was forced to fit the same template for the brain with larger ventricles (shown on the right). Voxel-wise comparisons of RAVENS maps can be performed using voxel-wise statistical tests.

quantify shape and local volumetric differences between individuals or groups, via statistical comparisons of shape transformations that map an atlas to individual anatomies. These approaches can potentially yield a very precise and local description of shape. However, their accuracy is limited by the accuracy of the underlying shape transformation, not only in terms of warping the template to the individual, but also in terms of establishing correct point correspondences between the template and the individual. Measuring the accuracy of these approaches remains an active research area, despite the rapid progress in the field of 3D deformable registration during the past several years (Gee *et al.*, 1993; Christensen *et al.*, 1994, 1997; Collins *et al.*, 1994; Friston *et al.*, 1995b; Thompson and Toga, 1996; Davatzikos, 1996a, 1997; Thirion, 1998; Freeborough and Fox, 1998; Chen *et al.*, 1998; Wang and Staib, 1999). Somewhat related to these methods is landmark-based morphometry (Bookstein, 1989; Rangarajan and Duncan, 1998), although it is based on isolated landmarks rather than continuous transformations.

A current limitation of methods based on shape transformations is that they are very sensitive to the accuracy of the underlying shape transformation. Although this is not a limitation of the conceptual framework behind measuring shape transformations, it is a limitation in practice. For example, a relatively simple polynomial transformation can align brain structures across subjects reasonably well. However, although the residual variability can be visually interpreted as small, this residual variability may be precisely what can ultimately identify subtle and localized effects of disease on brain morphology, if the properties of the underlying shape transformations are used for this analysis. Methods that attempt to overcome this limitation based on very high-dimensional elastic or fluid transformations have been proposed (Thompson and Toga, 1996; Davatzikos, 1997; Christensen *et al.*, 1997). Recent attempts to improve the accuracy of point correspondences of high-dimensional transformations by incorporating geometric information in the deformation engine were presented in Shen and Davatzikos (2000a,b) and Davatzikos (2001).

The second family of methods perform regional volumetric analysis of brain, gray, or white matter densities, after spatial normalization. The method examined in this paper falls under this category and is referred to as regional analysis of volumes examined in normalized space (RAVENS); it was described in Goldszal *et al.* (1998) and Davatzikos (1998) and later applied for analysis of cross-sectional and longitudinal analysis of age effects (Resnick *et al.*, 2000). Related to this approach is the method of voxel-based morphometry (VBM) (Ashburner and Friston, 2000; Woermannn *et al.*, 1999). RAVENS and VBM are based on the spatial normalization of volumetric images into a stereotaxic space, followed by a subsequent voxel-wise statistical analysis of the resulting spatial distributions of gray matter (GM), white matter (WM), and cerebrospinal fluid (CSF). Local atrophy can be detected in these methods if it significantly changes the spatial distribution of GM, WM, and CSF. Although RAVENS and VBM are concerned only with local volumetric measurements and do not measure any higher order shape characteristics, they are less sensitive to spatial normalization errors in comparison with methods based on displacement fields.

While RAVENS and VBM approaches are related, they are different in two ways. The first difference is in the spatial normalization transformation. RAVENS uses a very high dimensional elastic transformation, referred to as spatial transformation algorithm for registration (STAR). STAR is driven by point correspondences established on distinct anatomical surfaces, such as the cortex, sulci, gyri, and boundaries of subcortical structures and the ventricles. VBM relies on relatively smoother parametric transformations (Ashburner *et. al.*, 1998). The second difference is in the way in which the spatial distributions of GM, WM, and CSF in the stereotaxic space are determined. In VBM, global shape differences are eliminated via relatively low-parameter shape transformations (Ashburner *et. al.*, 1998), and differences in the residual variability

are examined via SPM analysis. Residual variability, however, is difficult to interpret, since it is intimately linked to registration error of the underlying spatial normalization method. Most importantly, even if it is assumed that differences in residual variability are somewhat linked to group differences in morphology, *a precise quantification of the volumetric group differences in GM, WM , or CSF, or of longitudinal rates of atrophy, requires that volumetric units are preserved during the spatial transformation*. RAVENS maps preserve the volumes of different tissues both at the local and at the global level, as described in the following section (Goldszal *et al.*, 1998; Davatzikos, 1998). Therefore, local group comparisons of RAVENS maps are exactly equivalent to volumetric comparisons of the original images (prior to spatial normalization) in the respective regions. Moreover, an exact quantification of longitudinal atrophy is readily obtained via the RAVENS analysis.

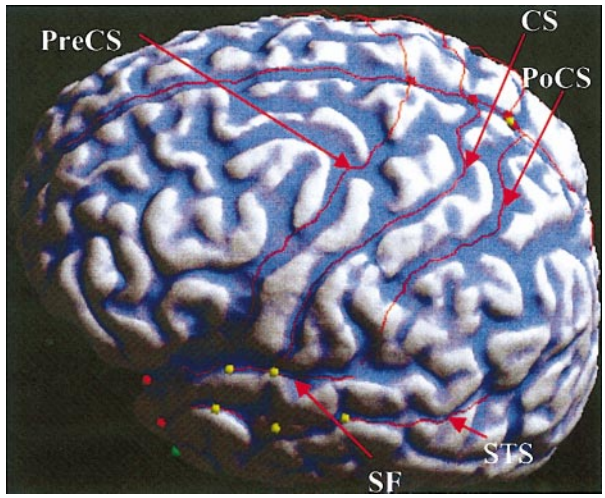

FIG. 2. An example of the curves used as constraints in the spatial normalization. High curvature regions are shown dark. The sulci shown are the precentral sulcus (PreCS), the central sulcus (CS), the postcentral sulcus (PoCS), the Sylvian fissure (SF), and the superior temporal sulcus (STS). These curves are parameterized by piece-wise constant speed parameterizations (uniform stretching) in-between breakpoints (yellow boxes). Breakpoints are typically placed on recognizable landmarks and also on or near intersections of sulci.

METHODS

Simulation of Atrophy

To investigate whether the RAVENS analysis can detect highly localized atrophy, we generated simulated images, based on T1-weighted SPGR images of 11 normal elderly subjects (average age was 70.1, with standard deviation 5.9). In particular, we selected two target gyri, namely the right precentral gyrus (PCG) and the left superior temporal gyrus (STG), in all subjects. Based on triplanar displays of these images, we manually defined these gyri using the *Display* software package that is freely distributed by the Brain Imaging Center, Montreal Neurological Institute. We subsequently introduced a 30% uniform contraction into the labeled gyri, thereby creating an additional 11 images with very localized atrophy in the two specific gyri. This simulation experiment created the type of data that one expects in longitudinal studies, since the two groups being compared included the same subjects, with the difference between the two groups being the localized atrophy.

Spatial Normalization

To generate the RAVENS maps, we segmented all 22 images into GM, WM, and CSF. Our segmentation procedure employs a method based on Markov random fields, with inhomogeneity correction (Yan, 1995). This approach has been validated (Goldszal *et al.*, 1998) and produces highly reliable measures, as demonstrated in our longitudinal aging study (Resnick *et al.*, 2000). To allow voxel-based analysis, the segmented images were then spatially transformed into a common template, which was the skull- and cerebellum-stripped image of a single participant who had a moderate degree of ventricular atrophy and therefore represented a typical brain of this group. In principle, the analysis is independent of the template. However, in practice it is reasonable to choose a template that is representative of the group average, in order to reduce the effect of registration errors. This spatial normalization step was performed using STAR (Davatzikos, 1996, 1997; Vaillant and Davatzikos, 1999). STAR first fits deformable surfaces to the outer and inner boundaries of the brain, thus establishing a large number of point correspondences. These point correspondences are then interpolated everywhere else in the brain via a 3D elastic warping transformation.

In our current validation experiments, we employed a refined approach to the spatial normalization initially reported in (Davatzikos, 1996), establishing point correspondences in the cortex by drawing a number of parameterized curves along sulci and gyri bilaterally (as in Fig. 2). The curves that we defined in this paper were along the outer (exposed) edge of the following sulci: central, precentral, postcentral, superior-temporal, Sylvian, and interhemispheric fissures. Since a number of landmark points were defined along each of these curves, the resulting curve parameterizations had piece-wise constant speed, i.e., they correspond to a uniform stretching between landmark points. Typically, landmark points were placed on or near the intersections of curves corresponding to different sulci. The curve-to-curve mapping was then used to elastically reparameterize each subject's cortical surface, so that corresponding sulci have the same

parametric coordinates on the unit sphere, which serves as the parametric domain for each cortical surface (Davatzikos, 1996; Vaillant and Davatzikos, 1999). We emphasize that our approach differs significantly from fiducial-based approaches, such as that of Bookstein (1989), in which a number of manually defined point correspondences are used to find the 3D warping field. In particular, ventricular boundary matching is achieved fully automatically. Moreover, the outer cortical surface is found via a deformable surface algorithm and is used to guide the placement of the sulcal curves. Importantly, sulcal constraints are then used to reparameterize, i.e., regrid, this surface, thus generating a large number of point correspondences that constrain the warping transformation throughout the whole cortical surface and not only on the fiducials.

Generation of the RAVENS Maps

An important issue that arises when performing regional volumetric analysis in a stereotaxic space is that spatial normalization, by definition, changes the anatomy to be measured and therefore changes the resulting volumetric measurements. To address this issue, we generate the RAVENS maps in a way that preserves the volumetric measurements of each tissue, both locally and globally (Davatzikos, 1998; Goldszal *et al.*, 1998). This is accomplished by visiting every single voxel of a subject's image once and only once and mapping it, via the elastic transformation, to a target location in the stereotaxic space associated with the template. For each target location, there is one counter for each tissue, which is incremented accordingly each time a voxel is mapped to that location. Since a voxel is generally mapped to a location between grid vertices in the target image, the volume that it carries is mapped to the eight nearest grid vertices, with weights that are inversely proportional to distance. At the end of this procedure, it is guaranteed that the volume of each structure is equal to the integral of the RAVENS map within that structure. For example, the integral of the RAVENS maps of Fig. 1 provides the ventricular volumes of these subjects.

The mapping procedure described above implies that image intensity of the RAVENS maps encodes volume prior to elastic warping. For example, a RAVENS map with a relatively brighter precentral gyrus implies that relatively higher volume in that subject's precentral gyrus is forced to fit into the template's precentral gyrus. RAVENS maps have, in general, variable intensity distribution throughout the brain, reflecting the fact that different structures (including cortical structures) vary in volume across subjects.

To ensure fairness in the comparison with the VBM approach implemented through SPM, a global linear transformation was applied to all elastically warped images to place them into the SPM template space and to resample them at the same resolution.

Statistical Analysis

The RAVENS maps were smoothed by a Gaussian filter of different kernel sizes, varying from 5 to 15 mm, and then analyzed using the SPM'99 software to conduct a voxel-wise paired *t*-test analysis. Since the brightness of the RAVENS maps is proportional to volume, the RAVENS maps can be analyzed in a fashion similar to functional images (Ashburner and Friston, 2000). In the statistical analysis, effects were considered significant if the peak height was $P \leq 0.001$ (uncorrected) and cluster size was at least 20 voxels. Corrected values by SPM were also calculated.

Voxel-Based Morphometry

The main goal of this paper is to validate the RAVENS methodology on simulated images of longitudinal atrophy. For comparison purposes, however, we also examined the sensitivity of the commonly used SPM VBM approach (Ashburner and Friston, 2000) for detection of the simulated atrophy. In that approach, the MR images were first spatially normalized to the T1 template distributed with SPM'99. The transformation parameters were then applied to the same skull- and cerebellum-stripped images as were used in the RAVENS analysis. These spatially normalized images were then segmented into GM, WM, and CSF, using the SPM software. The GM and WM were combined to define brain tissue, which was subjected to statistical analysis by paired *t* tests, using procedures identical to those applied to the RAVENS maps. (The automated skull-stripping procedure implemented in SPM yielded poor results with our data, and thus, we used our semiautomated approach to skull-strip the images. This had the additional advantage of using the same initial images in our comparison of the RAVENS and VBM approaches.) Finally, we observed that one reason for the limited sensitivity of VBM (described under Results) was the lower resolution ($2 \times 2 \times 2$ mm) of the SPM template in comparison with the original images ($0.94 \times 0.94 \times 1.5$ mm). The lower resolution adversely affected the segmentation accuracy, most likely due to partial volume effects after reduction to lower resolution. Hence, we also tested a modified version of VBM, which we refer to as VBM2, in which skull-stripped images were first segmented at their original resolution using SPM and subsequently spatially normalized by using the spatial normalization parameters determined from the T1 images.

ROI-Based Analysis Revisited

Many structural and functional brain imaging studies have relied on ROI-based measurement methods.

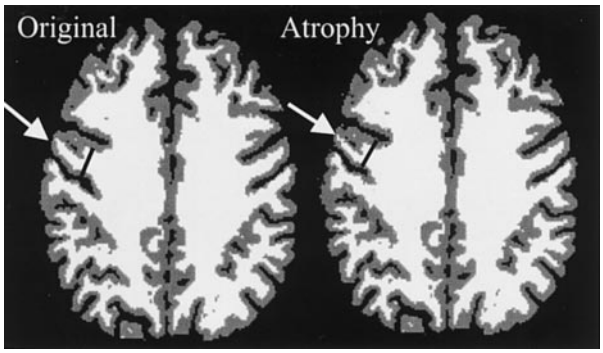

FIG. 3. An example of simulated atrophy in the precentral gyrus (indicated by arrows). A small black line of the same length has been added in both images as a reference for comparison of the thickness of the precentral gyri in the two images.

The main drawback of this approach is that it requires the manual definition of the regions of interest on every subject in the study, which may be unreliable and makes its use prohibitive when even a moderate number of images or ROIs is involved, because of time limitations. This limitation prompted the development of statistical parametric mapping methods, initially for functional imaging (Friston *et al.*, 1995a), and subsequently for structural imaging, as detailed in the Introduction. However, the concurrent development of more accurate spatial normalization methods can help overcome some of the limitations of ROI analysis, as detailed in this section.

Because of the constraints imposed by the parameterized sulcal curves, which were described earlier, STAR yields a good alignment of adjacent cortical gyri. Consequently, by averaging the RAVENS maps within a group under study, we obtain a fairly crisp definition of the anatomy of the group. Individual ROIs can then be defined based either on the average RAVENS maps or on the template used in the spatial normalization. By construction of the RAVENS maps, the integral of a subject's RAVENS map within any ROI is equal to the volume of the corresponding ROI in that subject's original image prior to spatial normalization. Therefore, an estimate of the volume of each ROI can be directly obtained. It is important to note that, in this approach, each ROI is defined only once for the whole group rather than for each individual subject. Therefore, the procedure requires far less human effort. Moreover, since the template is defined only once, this approach overcomes the reliability issues associated with the traditional ROI-based approach. We have previously validated this approach against manual tracings for several subcortical structures (Goldszal *et al.*, 1998).

To demonstrate the utility of this approach using our simulated images with selective cortical atrophy, we calculated volumes for the ROIs for the right precentral and left superior temporal gyri, after drawing them in the template. Volumetric measurements of these two gyri were obtained for all images by integrating the respective RAVENS maps within these ROIs. Finally, paired *t* tests were performed to compare volumetric estimates between the images without atrophy and the images with simulated atrophy.

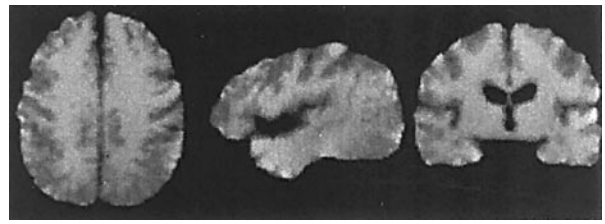

FIG. 4. Average RAVENS maps of brain tissue (GM and WM).

RESULTS

Detection of Simulated Atrophy

An example of an image with simulated atrophy is shown in Fig. 3. A transverse section of the segmented image at a level including the central sulcus is shown for a single subject before (left) and after (right) uniform contraction within the right precentral sulcus. This example illustrates the highly localized nature of the atrophy in the images on which the RAVENS and VBM approaches were tested.

In order to visually demonstrate the accuracy of the elastic spatial normalization used in RAVENS, we created an average image of the brain RAVENS maps. These average maps are shown in Fig. 4. In order to better show the accuracy of alignment of individual gyri and sulci by RAVENS, in Fig. 5 we show the average WM RAVENS map.

The ability of the RAVENS analysis to detect the regionally specific simulated atrophy was examined by voxel-wise paired *t* tests applied on the respective RAVENS maps. Results are shown in Fig. 6. It is evident that the paired *t*-test analysis detected significant differences in volumes for the two regions in which atrophy was simulated. To better visualize these results, in Fig. 7 we show volume renderings of the *t* statistic overlaid on the average brain RAVENS map. The renderings clearly show significant differences lo-

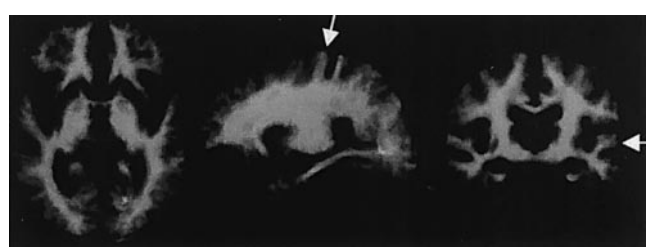

FIG. 5. The average white matter RAVENS map, demonstrating the accuracy of the spatial normalization (precentral and superior temporal gyri are indicated by arrows).

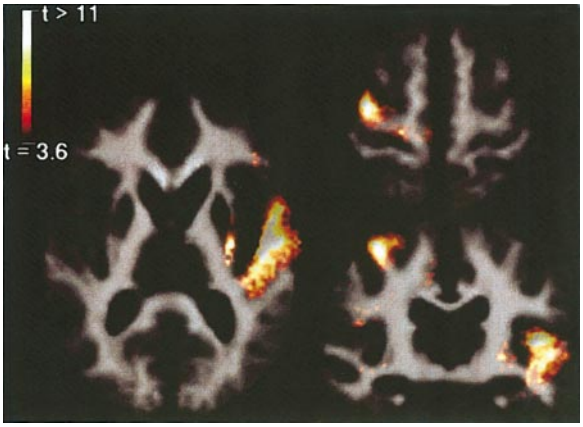

FIG. 6. Overlays of *t*-statistic maps and the average WM RAVENS map, demonstrating the detection of atrophy in the two gyri: PCG and STG. Only the white matter average map is shown, in order to better distinguish the gyral structure. Notice that the regions of significant atrophy extend into areas of gray matter. However, the most significant peaks, particularly after spatial filtering of the data, are in the centers of the gyri, i.e., primarily in white matter regions, as expected.

calized to the two regions of atrophy, the right precentral gyrus and left superior temporal gyrus.

ROI-Based Analysis Using the RAVENS Maps

Volume estimates of the right precentral gyrus and left superior temporal gyrus before and after the addition of simulated atrophy were compared by paired *t* tests. As shown in Table 1, ROI volumes determined using the RAVENS maps showed highly significant differences between original images and images with simulated atrophy. The substantially lower *P* values obtained via the ROI analysis of the RAVENS maps compared to the voxel-based analysis are indicative of the higher sensitivity of the former method relative to the latter. (Note that the same number of subjects was used in all measurements, and therefore differences in *P* values reflect differences in effect sizes.) This is due to the fact that voxel-wise measurements are very sensitive to noise and have greater variability, since they sample a very small region; they are also sensitive to registration errors, since the size of each voxel is comparable to, or even smaller than, the registration error. The high sensitivity of the ROI-based analysis is evident across a variety of comparisons. The left column of measurements in Table 1 reflects the result for *t* tests on the volumetric measurements obtained from the RAVENS maps directly. The second column presents the result based on a comparison of the ratios of the volumes from original and simulated images to unity, and the third column is analogous to the first, except the RAVENS maps were first normalized for global brain volume differences. Global brain volume for each image was determined from the integral of its RAVENS map.

TABLE 1

	Difference	Ratio	Normalized difference
Right precentral gyrus	1.3×10^{-8}	3.1×10^{-8}	5.5×10^{-8}
Left superior temporal gyrus	6.4×10^{-8}	2.5×10^{-6}	1.1×10^{-6}

Note. The *P* values of paired *t* tests on the integral of the RAVENS maps within ROIs delineating the right precentral gyrus and the left superior temporal gyrus, before and after simulated atrophy, are shown. The ROIs were drawn on the template brain, and the integral of the RAVENS maps within them was calculated, yielding an estimate of the volume of each ROI. The first column was obtained by considering the difference between the state without atrophy and the state with atrophy, the second column considered the ratios of the RAVENS integral in each ROI between the state with atrophy and the state without atrophy, and the third column was based on the differences of the first column, except that these differences were normalized for total brain volume.

Comparison with VBM

As explained under Methods, we compared the sensitivity to detect simulated atrophy for the RAVENS approach with the VBM and VBM2 methods of SPM. Figure 8 plots the maximum values of the *t* statistic for the RAVENS and VBM approaches in the clusters corresponding to the right PCG and left STG, the regions of simulated atrophy. Only regions detected with $P < 0.001$ (uncorrected) are included in this plot. Values of the paired *t* statistic are plotted as a function of the kernel size of the Gaussian filter used to smooth the data prior to statistical analysis. There is no curve in Fig. 8a for VBM, because VBM did not detect the simulated atrophy for the right precentral gyrus with uncorrected *P* values lower than 0.001. In general, the RAVENS analysis provided higher values of the *t* statistic, and it was robust with respect to the kernel of the Gaussian filter within realistic filter sizes.

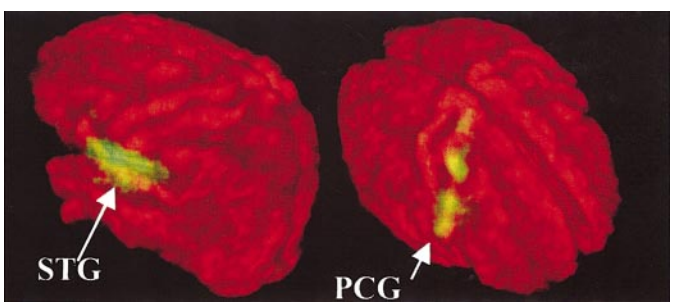

FIG. 7. Volume rendering of the *t* maps overlaid on the average RAVENS map of this group. The right precentral gyrus (PCG) and the left superior temporal gyrus (STG) were determined by the RAVENS analysis to display significant group differences, which is in agreement with the simulated atrophy. Values of the *t* statistic higher than 3.7 are displayed, for clarity. Notice that atrophy appears more spread out, due to the spatial filtering applied prior to statistical analysis.

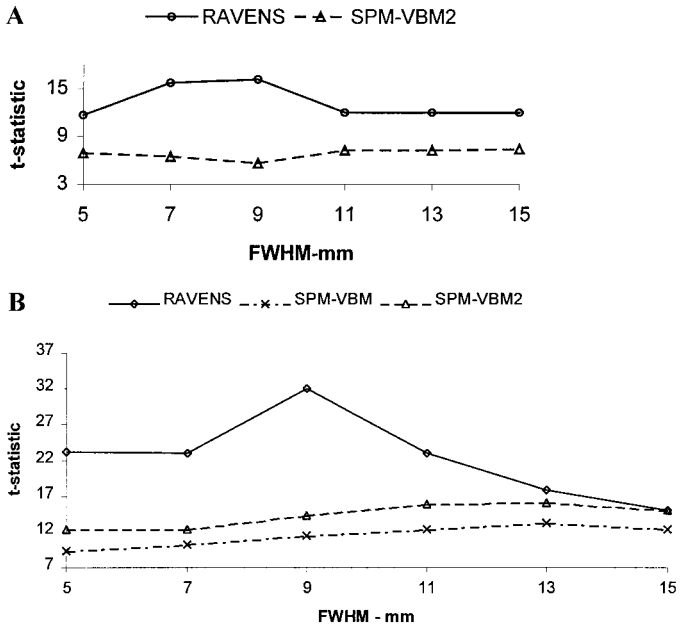

FIG. 8. Plots of the value of the *t* statistic at the peaks of clusters corresponding to (a) the precentral gyrus and (b) the superior temporal gyrus. SPM-VBM is the result of the method described in Ashburner *et al.* (2000), and SPM-VBM2 is its modification in which images are first segmented and then spatially normalized, thereby avoiding the effects of partial volume on the segmentation. RAVENS is the methodology described in this paper, which uses a feature-based elastic warping.

We also measured the corrected *P* values, as calculated by the SPM'99 correction for multiple comparisons performed based on the spatial smoothness of the data. For the 9-mm filter size, which was optimal for RAVENS, the corrected *P* values were 0.003 for STG and 0.24 for PCG. For the optimal kernel size for SPM (13 mm), the corresponding values were 0.21 (STG) and 1.0 (PCG). We note that *P* values in this study should be interpreted with caution. Our study was intended to (1) validate that relatively higher values of the RAVENS maps are found in the regions of atrophy, compared to the rest of the brain, and (2) compare the sensitivity of RAVENS with VBM. The *P* values in a real study will depend on the sample size, on the degree of atrophy, and on the shape and size of the region of atrophy.

DISCUSSION AND CONCLUSIONS

In this paper, we described an enhancement and further validation of a method for voxel-based morphology, referred to as regional analysis of volumes examined in normalized space. Adding manually defined constraints imposed by parametric curves and surfaces, we applied a flexible elastic 3D spatial normalization algorithm (STAR) to high-resolution images to create spatial maps of GM, WM, and CSF in a stereotaxic space. The parametric curves follow sulcal or gyral boundaries on the cortex. The elastic transformation guarantees that the volume of different tissues is preserved both locally and globally and therefore that the integral of a subject's RAVENS map of a particular tissue over any structure is equal to the volume of that tissue in that structure, prior to elastic warping. We validated this methodology using images from 11 elderly subjects, in which atrophy in two gyri was simulated, thus yielding 11 corresponding images with simulated atrophy. RAVENS was used to localize intraindividual differences in this sample of matched images. The main conclusions drawn from our experiments are as follows:

1. If appropriate cortical constraints are defined, the RAVENS maps provide adequate definition of the anatomy for highly localized effects to be detected via voxel-wise analysis. For example, constraints placed on the precentral, central, postcentral, and superior temporal sulci, as well as the lateral aspect of the Sylvian fissure, yielded a clear definition of the adjacent gyri in the RAVENS maps. In our simulation experiments, these definitions were sufficient to detect the simulated atrophy in the right precentral and left superior temporal gyri. While the specification of these limited additional sulcal constraints required manual definitions (about 20 min for a trained rater), we estimate that a more complete definition of sulcal constraints would require no longer than 45 min per subject (for 25–30 constraints).

2. Our experiments also demonstrated that a new form of ROI-based analysis, namely one using the RAVENS maps, can be performed without the need for parcellation of each brain individually. A single parcellation based on the template used in the spatial normalization is the only manual interaction required for the definition of ROIs. Integrating the values of the RAVENS maps within these ROIs directly yields regional volumetric measurements for each image. Standard statistical methods can then be applied on these ROI volumetric measurements. The fact that ROIs are defined only once renders this approach far more practical than traditional ROI analyses, which require the definition of ROIs on each subject's images. This approach is also attractive from a different perspective, since it dramatically reduces the effect of noise and registration errors, by integrating the RAVENS maps over an entire ROI. This was demonstrated experimentally with *P* values of the order of 10^{-6} and 10^{-8}, which are several orders of magnitude lower than those of voxel-wise *t* tests for the same image set. However, this approach suffers from the same limitation inherent in all region-based analyses—the requirement of *a priori* knowledge and specification of a particular ROI. Con-

sequently, if the predefined ROIs do not reflect the underlying regions of atrophy, the sensitivity of the approach will be reduced. In our experiments, a uniform contraction of the region was performed to define atrophy on the simulated images. In reality, atrophy may occur only in a localized part of a region, and this will result in a trade-off between sensitivity for the ROI and voxel-based analyses. Thus, the two approaches are optimally used in a complementary manner.

3. Using paired *t* tests, implemented within SPM'99, we were able to detect highly localized intraindividual differences in atrophy, via the RAVENS maps.

4. The RAVENS analysis performed considerably better than VBM across a range of smoothing kernels. The peak of the detection sensitivity was obtained with a 9-mm Gaussian filter, which roughly is the largest smoothing kernel that does not spill over into neighboring gyri. Of course, this would depend on the thickness of the particular gyrus. The relatively lower sensitivity of VBM is counterbalanced, to some extent, by the fact that VBM uses a fully automated procedure for spatial normalization.

In our study we used only a limited number of sulcal constraints, namely the ones close to the two gyri of interest. In our clinical studies, we use a larger number of sulcal constraints spanning the whole cortical region. This way, any cortical region is bounded by some sulcal curves. However, sensitivity of the RAVENS approach is bound to be relatively higher close to the curves used as constraints. Accordingly, more constraints should be placed close to regions that are of interest in a particular study.

Our initial studies of the accuracy of the RAVENS approach for analysis of localized brain atrophy yielded encouraging results. However, the validation procedure of this study is limited, as it was not possible to examine all possible scenarios of atrophy. For example, we introduced uniform atrophy within brain tissue and did not differentiate between gray and white matter. One could introduce a variable rate of atrophy within the two gyri we used in this work, perhaps by sampling a statistical distribution, and a different degree of atrophy in white and gray matter. One could also vary the size of the region within which atrophy was introduced or vary other pertinent parameters. The purpose and scope of the current paper was to demonstrate that RAVENS maps can accurately detect a highly localized region of brain atrophy. Undoubtedly, the ability of the RAVENS analysis to detect localized atrophy in real data sets will depend on the size, the magnitude, and the spatial pattern of this atrophy, as well as on its variability across subjects and on the sample size.

A current limitation of our approach to spatial normalization is the need for manual definition of sulcal or gyral curves that are used as constraints in the elastic warping. To its advantage, SPM's spatial normalization method is fully automated. However, extensions of our approach to automatically identify major sulci are possible. In particular, we have previously presented an approach using spatial probability distributions of the sulci on the unit sphere as priors used by an automated sulcal recognition algorithm (Vaillant, 1999). We are currently extending this approach to sulci defined on spherical maps of the outer and full cortical surfaces (Tao *et al.*, 2000), with very promising results.

Although several directions merit further investigation, our experiments demonstrated that the current form of RAVENS analysis is a useful tool in neuroimaging studies. These tools are being applied for investigation of cross-sectional and longitudinal age effects on brain morphology.

ACKNOWLEDGMENTS

This work was supported in part by NIH Contract NIH-AG-93-07 and NIH Grant R01-AG14971.

REFERENCES

Ashburner, J., Hutton, C., Frackowiak, R., Johnsrude, I., Price, C., and Friston, K. 1998. Identifying global anatomical differences: deformation-based morphometry. *Hum. Brain Mapp.* **6:** 348–357.

Ashburner, J., and Friston, K. J. 2000. Voxel-based morphometry: The methods. *NeuroImage* **11:** 805–821.

Bookstein, F. L. 1989. Principal warps: Thin-plate splines and the decomposition of deformations. *IEEE Trans. Pattern Anal. Mach. Intell.* **11:** 567–585.

Briquer, L. L., and Gee, J. C. 1997. Design of a statistical model for brain shape. *Lect. Notes Comp. Sci.:Proc. Inform. Proc. Med. Imaging* **1230:** 477–482.

Chen, M., Kanade, T., Rowley, H. A., and Pomerleau, D. 1998. Quantitative study of brain anatomy. In *Proc. Biomed. Image Anal. Workshop,* pp. 84–92.

Christensen, G. E., Rabbitt, R. D., and Miller, M. I. 1994. 3D brain mapping using a deformable neuroanatomy. *Phys. Med. Biol.* **39:** 609–618.

Christensen, G. E., Joshi, S. C., and Miller, M. I. 1997. Volumetric transformation of brain anatomy. *IEEE Trans. Image Process.* **16:** 864–877.

Collins, D. L., Neelin, P., Peters, T. M., and Evans, A. C. 1994. Automatic 3D inter-subject registration of MR volumetric data in standardized Talairach space. *J. Comput. Assisted Tomogr.* **18:** 192–205.

Collins, D. L., Zijdenbos, A. P., Baare, W. F. C., and Evans, A. C. 1999. ANIMAL+INSECT: Improved cortical structure segmentation. In *Proc. Inform. Process. Med. Imaging,* IPMI'99, pp. 210–223.

Davatzikos, C. 1996. Spatial normalization of 3D brain images using deformable models. *J. Comput. Assisted Tomogr.* **20:** 656–665.

Davatzikos, C. 1997. Spatial transformation and registration of brain images using deformable models. *Comput. Vision Image Understand.* **66:** 207–222.

Davatzikos, C. 1998. Mapping of image data to stereotaxic spaces: Applications to brain mapping. *Hum. Brain Mapp.* **6:** 334–338.

Davatzikos, C. 2001. Measuring biological shape using geometry-based shape transformations. *Image Vision Comput.* **19:** 63–74.

Davatzikos, C., Vaillant, M., Resnick, S., Prince, J. L., Letovsky, S. I., and Bryan, R. N. 1996. A computerized method for morphological analysis of the corpus callosum. *J. Comput. Assisted Tomogr.* **20:** 88–97.

Davatzikos, C., and Resnick, S. M. 1998. Sex differences in interhemispheric connectivity: Correlations with cognition in women but not in men. *Cereb. Cortex* **8:** 635–640.

Ferrant, M., Warfield, S. K., Guttmann, C. R. G., Mulkern, R. V., Jolesz, F. A., and Kikinis, R. 1999. 3D matching using a finite element based elastic deformation model. In *Proc. MICCAI'98,* pp. 202–209.

Freeborough, P. A., and Fox, N. C. 1998. Modeling brain deformations in Alzheimer's disease by fluid registration of serial MR images. *J. Comput. Assisted Tomogr.* **22:** 838–843.

Friston, K. J., Holmes, A. P., Worsley, K. J., Poline, J. P., Frith, C. D., and Frackowiak, R. S. J. 1995a. Statistical parametric maps in functional imaging: A general linear approach. *Hum. Brain Mapp.* **2:** 189–210.

Friston, K. J., Ashburner, J., Frith, C. D., Poline, J. B., Heather, J. D., and Frackowiak, R. S. J. 1995b. Spatial registration and normalization of images. *Hum. Brain Mapp.* **2:** 165–189.

Gaser, C., Volz, H. P., Kiebel, S., Riehemann, S., and Sauer, H. 1999. Detecting structural changes in whole brain based on nonlinear deformations—Application to schizophrenia research. *NeuroImage* **10:** 107–113.

Gee, J. C., Reivich, M., and Bajcsy, R. 1993. Elastically deforming 3D atlas to match anatomical brain images. *J. Comput. Assisted Tomogr.* **17:** 225–236.

Goldszal, A., Davatzikos, C., Pham, D. L., Yan, M. X. H., Bryan, R. N., and Resnick, S. M. 1998. An image processing protocol for qualitative and quantitative volumetric analysis of brain images. *J. Comput. Assisted Tomogr.* **22:** 827–837.

Guimond, A., Meunier, J., and Thirion, J. P. 2000. Average brain models: A convergence study. *Comput. Vision Image Understand.* **77:** 192–210.

Machado, A. M. C., Gee, J. C., and Campos, M. F. M. 2000. A factor analytic approach to structural characterization. In *Proc. Workshop Math. Methods Biomed. Image Anal.,* pp. 219–225.

Miller, M. I., Christensen, G. E., Amit, Y., and Grenander, U. 1993. Mathematical textbook of deformable neuroanatomies. *Proc. Natl. Acad. Sci. USA* **90:** 11944–11948.

Miller, M., Banerjee, A., Christensen, G., Joshi, S., Khaneja, N., Grenander, U., and Matejic, L. 1997. Statistical methods in computational anatomy. *Stat. Methods Med. Res.* **6:** 267–299.

Rangarajan, A., and Duncan, J. S. 1998. Matching point features using mutual information. In *Proc. Biomed. Image Anal. Workshop,* pp. 172–181.

Resnick, S. M., Goldszal, A. F., Davatzikos, C., Golski, S., Kraut, M. A., Metter, E. J., Bryan, R. N., and Zonderman, A. B. 2000. One year changes in MRI brain volumes in older adults. *Cereb. Cortex* **10:** 464–472.

Shen, D., and Davatzikos, C. 2000a. An adaptive focus deformable model using statistical and geometric information. *IEEE Trans. Pattern Anal. Mach. Intell.* **22:** 906–913.

Shen, D., and Davatzikos, C. 2000b. Adaptive-focus statistical shape model for segmentation of 3D MR structures. In *Proc. MICCAI'2000,* pp. 206–214.

Tao, X., Etteman, M., Prince, J. L., and Davatzikos, C. 2000. Probabilistic maps of cortical sulci on spherical maps. In *Inform. Process. Med. Imaging, IPMI2000,* Davis, California, pp. 475–487.

Thirion, J. P. 1998. Image matching as a diffusion process: An analogy with Maxwell's demons. *Med. Image Anal.* **2:** 243–260.

Thompson, D. W. 1917. *On Growth and Form*. Cambridge Univ. Press, Cambridge, UK.

Thompson, P., and Toga, A. W. 1996. A surface-based technique for warping three-dimensional images of the brain. *IEEE Trans. Med. Imaging* **15:** 402–417.

Thompson, P. M., MacDonald, D., Mega, M. S., Holmes, C. J., Evans, A. C., and Toga, A. W. 1997. Detection and mapping of abnormal brain structure with a probabilistic atlas of cortical surfaces. *J. Comput. Assisted Tomogr.* **21:** 567–581.

Thompson, P. M., Woods, R. P., Mega, M. S., and Toga, A. W. 2000. Mathematical/computational challenges in creating deformable and probabilistic atlases of the human brain. *Hum. Brain Mapp.* **9:** 81–92.

Vaillant, M., and Davatzikos, C. 1999. Hierarchical matching of cortical features for deformable brain image registration. Lecture notes in *Comp. Sci.: Inform. Proc. in Med. Imaging* **1613:** 182–195.

Wang, Y., and Staib, L. H. 1999. Elastic model-based non-rigid registration incorporating statistical shape information. *Lect. Notes Comput. Sci.: MICCAI'98,* **1496:** 1162–1173.

Woermann, F. G., Free, S. L., Koepp, M. J., Ashburner, J., and Duncan, J. S. 1999. Voxel-by-voxel comparison of automatically segmented cerebral gray matter—A rater-independent comparison of structural MRI in patients with epilepsy. *NeuroImage* **10:** 373–384.

Yan, M. X. H., and Karp, J. S. 1995. An adaptive Bayesian approach to three-dimensional MR image segmentation. In *Proc. of Conf. on Inform. Proc. in Med. Imaging, IPMI'95,* pp. 201–213.